

Chapter 3

Experimental and theoretical study of chemical modification on chitosan

Abstract

This study presents both experimental and theoretical investigations into the modification of CS using BPB. Various techniques, such as FT-IR, UV/Vis, NMR, XRD, SEM, TGA, and DSC analysis, were employed for the analysis of both pure CS and MCS to establish the structure-property relationship. The antibacterial effectiveness of both CS and MCS against both gram-positive (*Bacillus subtilis*) and gram-negative (*Escherichia coli*) bacteria was investigated. The results revealed that MCS demonstrated superior antibacterial properties compared to pure CS. Moreover, a theoretical exploration was conducted to examine the reaction pathways involved in the chemical modification of CS by BPB using B3LYP functional for quantum chemical analysis.

3.1. Introduction

The growing environmental concern has sparked significant interest in the utilization of natural polysaccharides for various applications [109]. Natural polysaccharides are excellent choices for crafting innovative biomaterials due to their biocompatibility, renewability and lack of toxicity [62]. CS is a polysaccharide, in which D-glucosamine units are linked via β (1-4) linkage [110]. Due to its outstanding biocompatibility, non-toxicity and biodegradability, this material is being used in a variety of applications e.g., biotechnology, wastewater purification, functional food, biomedical, agriculture, environmental protection etc. [35]. CS is obtained from chitin, another biopolymer sourced from the protective outer coverings of various marine and terrestrial arthropods [111]. The extraction of chitin from marine sources is accomplished by a two-step process: deproteinization and demineralization [112]. Deacetylation of this extracted chitin results CS. Figure 1.7. shows the functional groups present in CS. These groups (amino and hydroxyls) provide opportunities for chemical modifications and may be used to tune the physicochemical properties of CS [113].

However, owing to the presence of extensive hydrogen bonding, both intermolecular and intramolecular, pristine CS is not soluble in any organic solvent. It is soluble only in an acidic aqueous solution. This restricts its applicability as an efficient flocculant. Therefore, it is necessary to improve the solubility profile of CS. Chemical modification is a way to improve its solubility [114-116]. Chemical modification via grafting may be a suitable strategy to maintain a hydrophilic–lipophilic balance in the CS too. For this, the functional groups present in the CS are converted to act as a site for grafting. The required amount of

material in the form of a polymeric chain may be grafted to the CS moiety using those active sites. The CS moiety with such active sites would be acting like a macroinitiator during the graft copolymerization [64]. There have been several reports on the chemical modification of CS aiming for various purposes [59-63].

Here we report the modification of CS with BPB aiming for further modification via grafting. The chemically modified CS and the pure CS were subjected to comprehensive analysis employing a variety of analytical techniques, including FT-IR, UV/Vis, NMR, XRD, SEM, TGA and DSC. Furthermore, the antibacterial activity of both CS and MCS against both *Escherichia coli* and *Bacillus subtilis* bacteria was assessed. Moreover, an attempt was made to find out the probable reaction pathways during the chemical modification of CS employing the quantum chemical analysis. The experimental results were tried to correlate with the theoretical findings. To the best of our knowledge, there is no such report available, that attempts to correlate the experimental results with the theoretical findings on the chemical modification of CS.

3.2. Synthesis

3.2.1. Chemically modified chitosan

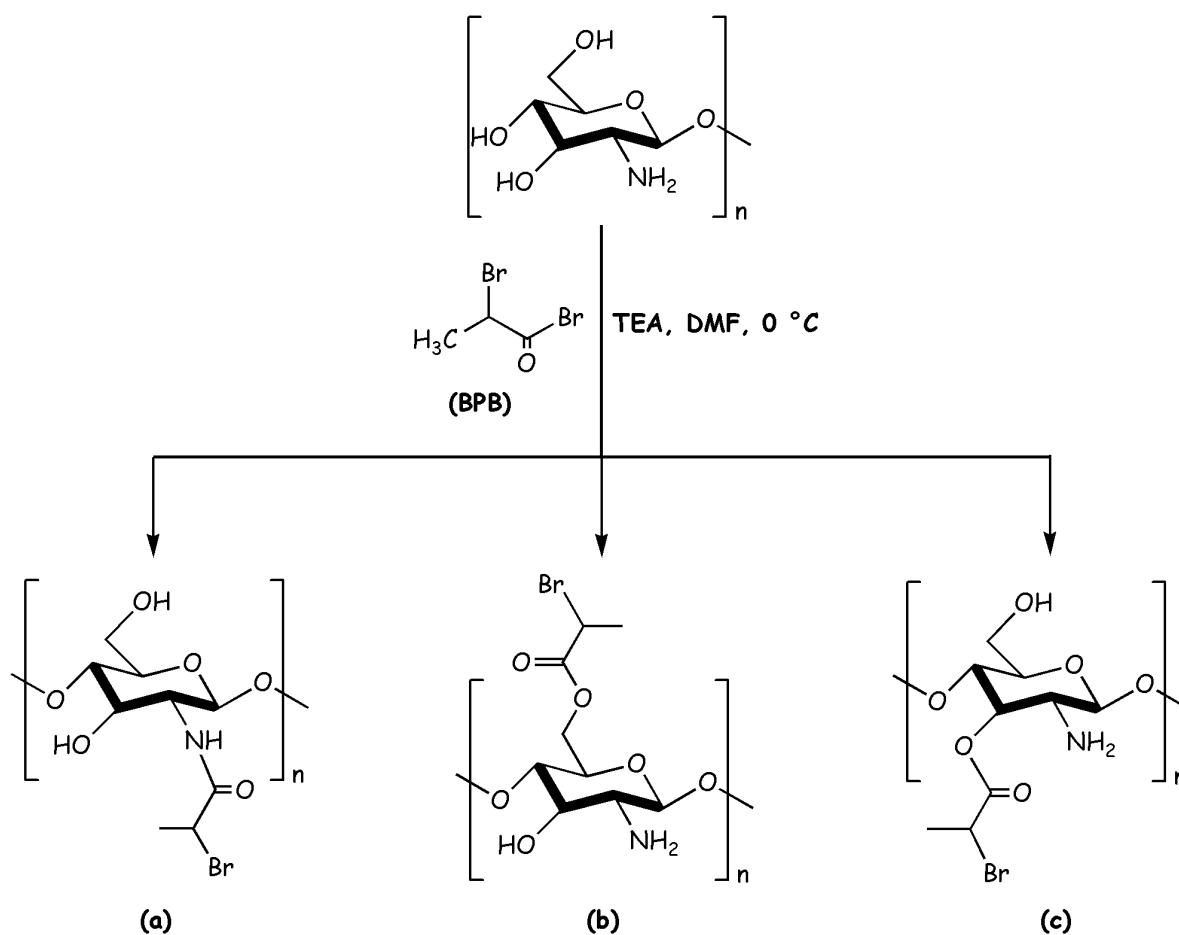
Modified chitosan (MCS) was synthesized through a single-step process using BPB, TEA, and DMF as the solvent.

In this process, 5 g of CS was dissolved in 20 g of DMF for 3 h at room temperature while being stirred magnetically. Following this, TEA (3 g, 0.0296 mol) was added at 0 °C and allowed to stir for 45 min. Subsequently at 0 °C, BPB (3 g, 0.0139 mol) was introduced dropwise while being continuously stirred.

After that, the mixture was left to react at room temperature for 24 h while being mechanically stirred. The mixture was then filtered and washed with deionized water. The filtrate was then vacuum-dried for 24 h at 70 °C.

The BPB attacked the CS matrix via amine group or primary hydroxyl group or secondary hydroxyl group.

The single-step preparation of MCS using BPB and TEA in DMF and its possible structures is illustrated in Scheme 3.1.



Scheme 3.1. Possible reaction scheme for preparing MCS. BPB attacked in (a) amine group (b) primary hydroxyl group and (c) secondary hydroxyl group.

3.2.2. Crude sample for Antibacterial Study

10 mg mL⁻¹ of 2% acetic solution was used to dissolve CS and MCS. For 5 h, the final solutions were continuously rotated at 40 °C in an even layer. The samples were then used to evaluate the antibacterial activity.

3.3. Results and discussion

3.3.1. Structural evaluation

3.3.1.1. Analysis via FT-IR spectroscopy

The FT-IR spectra of CS and MCS exhibit absorption bands within the 4000-700 cm⁻¹ range, as illustrated in Figure 3.1. Figure 3.1. highlights distinctions between the spectrum of CS and the characteristic absorption peaks of MCS. For CS, a pronounced band in the 3347-

3281 cm^{-1} range signifies N-H and O-H stretching, along with intramolecular hydrogen bonds. After the formation of MCS, these absorption peaks no longer persisted [61, 117].

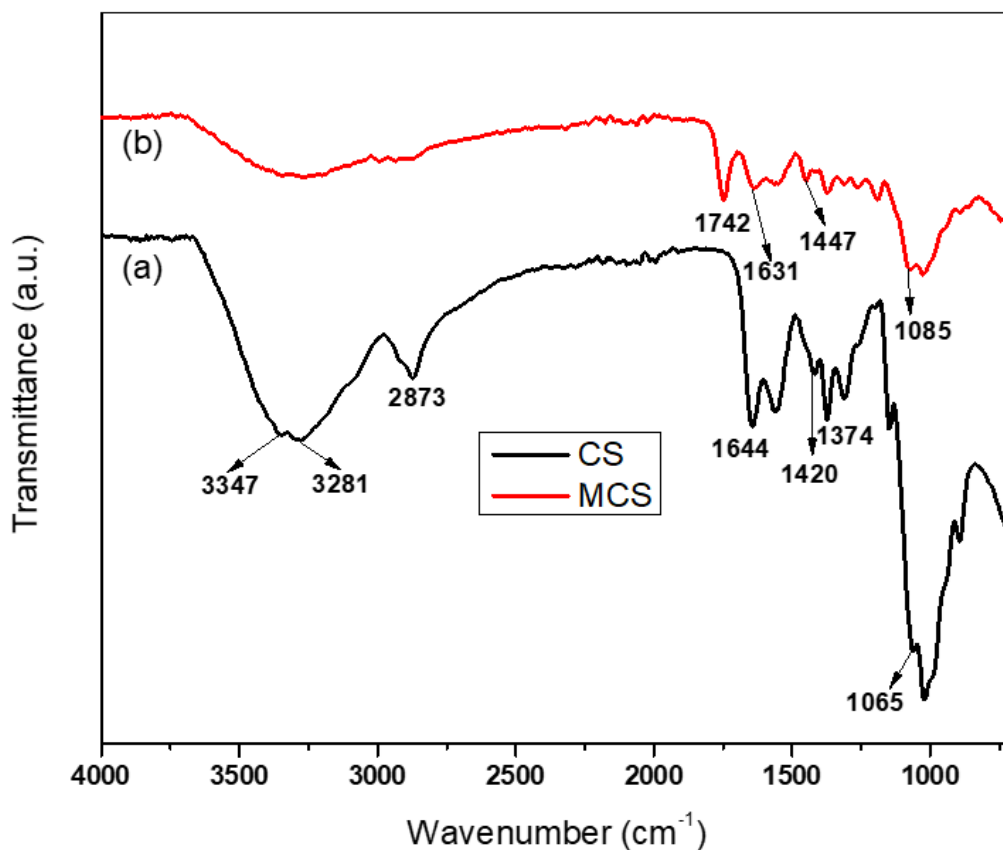


Figure 3.1. FT-IR spectra of CS and MCS.

The absorption peak associated with the secondary -OH groups on the CS molecule at 1065 cm^{-1} experienced a shift to 1085 cm^{-1} in the MCS molecule, suggesting that the secondary -OH group of CS molecules underwent a reaction with BPB. The -NH₂ in the CS molecule is responsible for the absorption peak at 1644 cm^{-1} ; in the MCS molecule, this peak has moved to a lower wavenumber, 1631 cm^{-1} . The observed shift signifies the participation of the amino group of CS in the reaction. [118]. In the instance of MCS, a novel carbonyl peak appeared at 1742 cm^{-1} , suggesting that BPB was successfully grafted onto CS [61].

3.3.1.2. Analysis via UV/Vis spectroscopy

As shown in Figure 3.2., the UV/Vis spectra of CS and MCS were obtained at ambient temperature. Absorption bands were noticeable in the 200-800 nm range for both CS and MCS. As depicted in Figure 3.2., CS does not exhibit any discernible absorption peak in the

450–650 nm wavelength region [119]. In contrast, MCS displays a wide absorption band centred at 564 nm. This signifies the reaction of CS with BPB takes place.

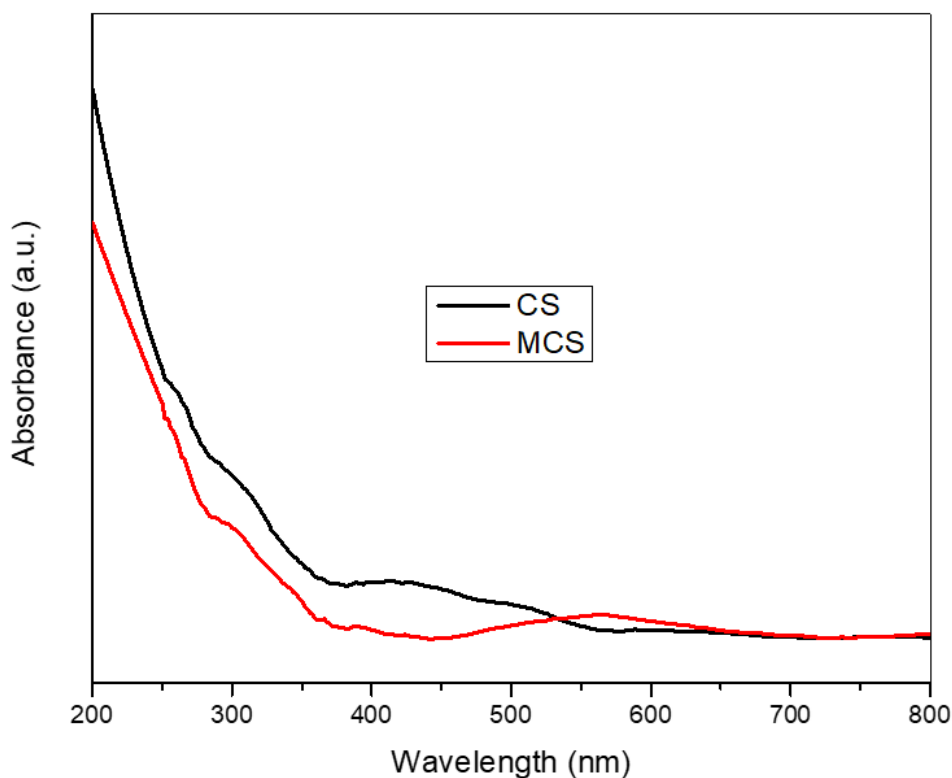


Figure 3.2. UV/Vis spectra of CS and MCS.

3.3.1.3. Analysis via NMR spectroscopy

Solid-state NMR provided additional insights into the chemical modification of CS by BPB. Figure 3.3. illustrates ^{13}C -NMR spectra of both CS and MCS. In the CS spectrum, the carbonyl carbon and methyl carbons of the N-acetyl group were observed at 175.25 and 23.93 ppm, respectively. The original CS exhibited a C=O peak at 175.25 ppm, but after BPB modification, two distinct peaks emerged in this region (at 170.51 and 174.97 ppm). The appearance of the peak at 170.51 ppm suggests the presence of the carbonyl carbon from BPB, possibly indicating grafting through the N-atom [120]. Another new signal appeared at 17.40 ppm, assigned to the methyl carbons of BPB. Additionally, the CS signal at 23.93 ppm shifted to 24.07 ppm in MCS, attributed to the deshielding effect of the bromine (Br) atom.

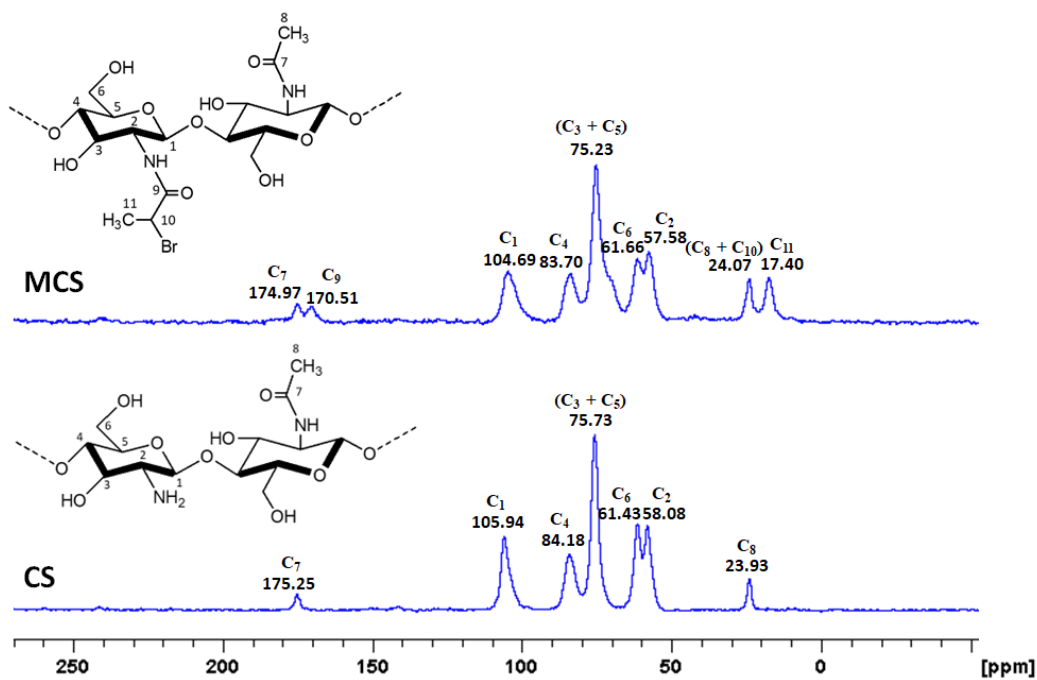


Figure 3.3. NMR Spectra of CS and MCS.

3.3.2. Morphological study

3.3.2.1. Analysis via XRD

The XRD patterns of MCS and CS are shown in Figure 3.4.

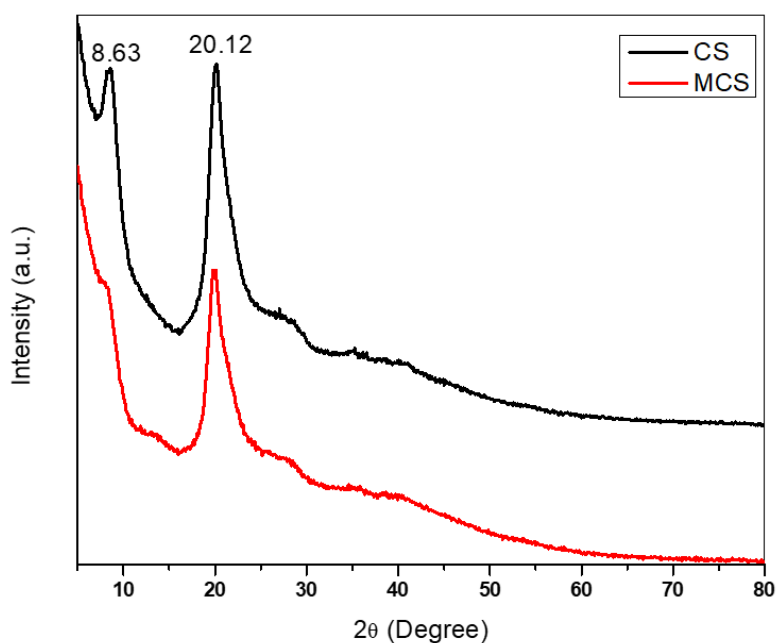


Figure 3.4. XRD diffractogram of CS and MCS.

Peaks at $2\theta = 8.63^\circ$ and $2\theta = 20.12^\circ$ were observed in the XRD pattern of CS. In the instance of MCS, the XRD pattern showed a single peak at around $2\theta = 20^\circ$. Nevertheless, in the case of MCS, the peak initially observed at $2\theta = 8.63^\circ$ vanished, and there was a decrease in the intensity of the peak at $2\theta = 20.12^\circ$ compared to CS. These findings indicate favorable compatibility with CS. Based on Figure 3.4., it can be inferred that the introduction of the BPB group induces an alteration in the crystallinity of CS. This change is likely influenced by factors such as π - π stacking, steric hindrance and hydrophobic forces [110].

3.3.2.2. Analysis via SEM

SEM images were acquired for CS and MCS to examine their respective morphologies. To achieve higher resolution, images were captured at a magnification of 1000X. The micrographs presented in Figure 3.5. illustrate the alterations in the morphologies of both CS and MCS. The SEM micrographs revealed a notable contrast in the surface of CS before and after modification. The analysis indicates that the surface of pure CS exhibited a smooth and irregular texture, whereas the MCS displayed a fibrous-like structure with a rough surface, accompanied by the presence of numerous particles on the surface [121]. The surface roughness of the MCS was found to be higher than that of the pure CS. This observation can be elucidated as an outcome of the interaction between the amine or hydroxyl groups of CS and BPB, likely leading to the disruption of hydrogen bonds existing in CS. Consequently, the interplay between CS and BPB induces noteworthy alterations in the surface morphology and crystallinity of CS [110].

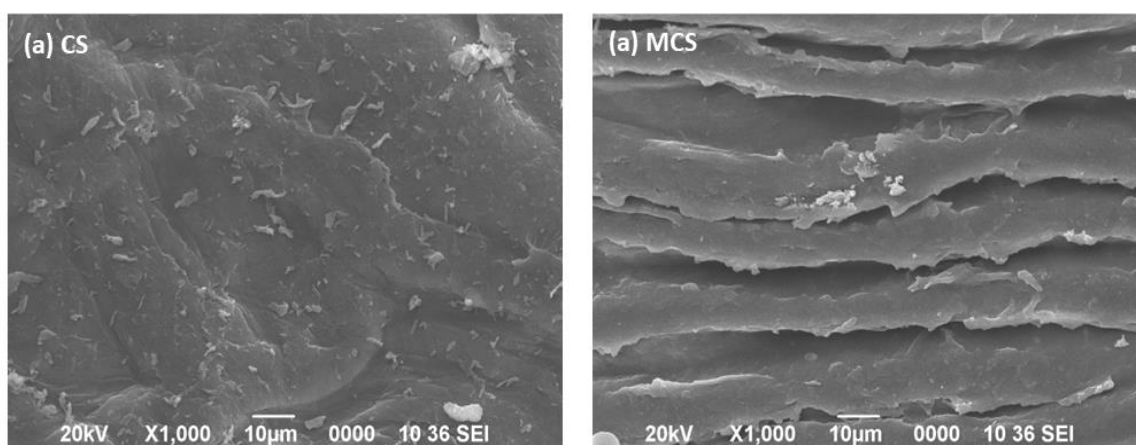


Figure 3.5. SEM micrographs of (a) CS and (b) MCS.

3.3.3. Thermal analysis

3.3.3.1. TGA

The TGA analysis profile as represented in Figure 3.6. shows different stages of weight loss over the selected temperature ranges for CS and MCS. Table 3.1. provides the key thermal attributes extracted from the TGA curves, including the onset temperature of the degradation process (T_{onset}) and the temperature at which maximum mass loss occurs (T_{max}).

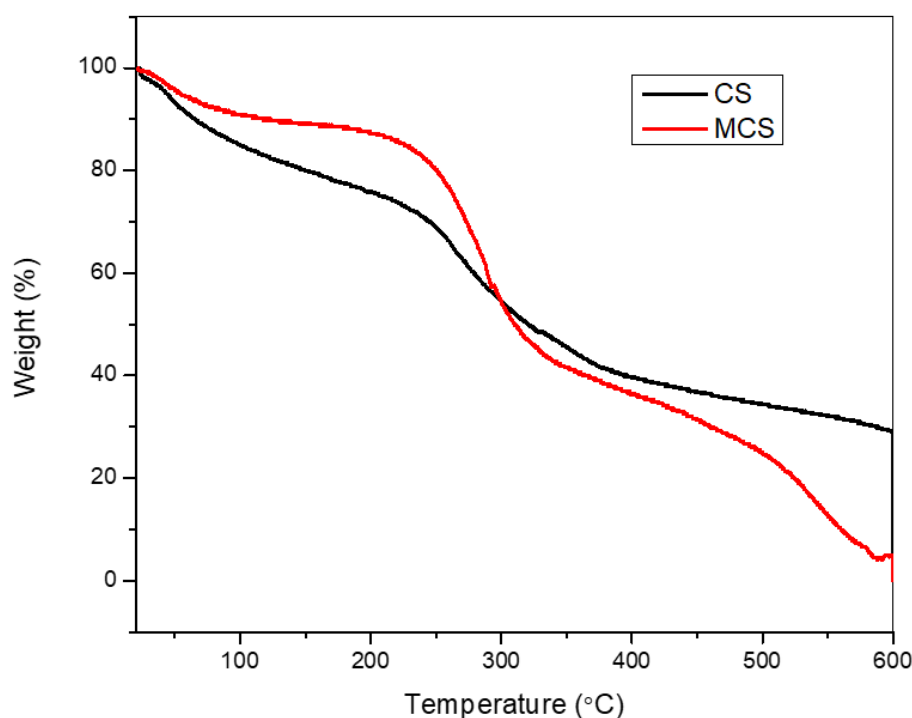


Figure 3.6. TGA plots of CS and MCS.

Two phases of weight loss are evident in the obtained TGA curves for CS and MCS. The initial phase reveals a slight decrease in weight between 30-107 °C, with this temperature range corresponding to the process of dehydration. The second thermal decomposition zone, occurring between 238-391 °C for CS, aligns with the primary pyrolysis and vaporisation of chemicals arising from the thermal breakdown of polymeric CS chains. As for MCS, the second phase of mass loss occurs in the temperature span of 228-337 °C. In accordance with certain authors [110, 119], the initial step is linked to the depolymerization and deacetylation of CS, while the subsequent stage related to the remaining cross-linked disruption of CS. The second stage degradation is caused due to oxidative degradation as confirmed from the exothermic peak around 304 °C (Figure 3.6.).

TGA analysis indicates that, in comparison to pure CS, MCS shows less thermal stability. The crystalline structure of these materials may be the cause of this finding. Certainly, MCS exhibits reduced crystallinity in comparison to pure CS, as depicted in Figure 3.4.

Table 3.1. Thermal characteristics of CS and MCS.

Sample	Degradation Temperature (°C)	
	T _{onset}	T _{max}
CS	238	391
MCS	228	337

3.3.3.2. Analysis via DSC

The DSC thermograms for CS and MCS are represented in Figure 3.7. show the initial endothermic peaks observed in both thermograms as a result of the water loss from the polymer backbone.

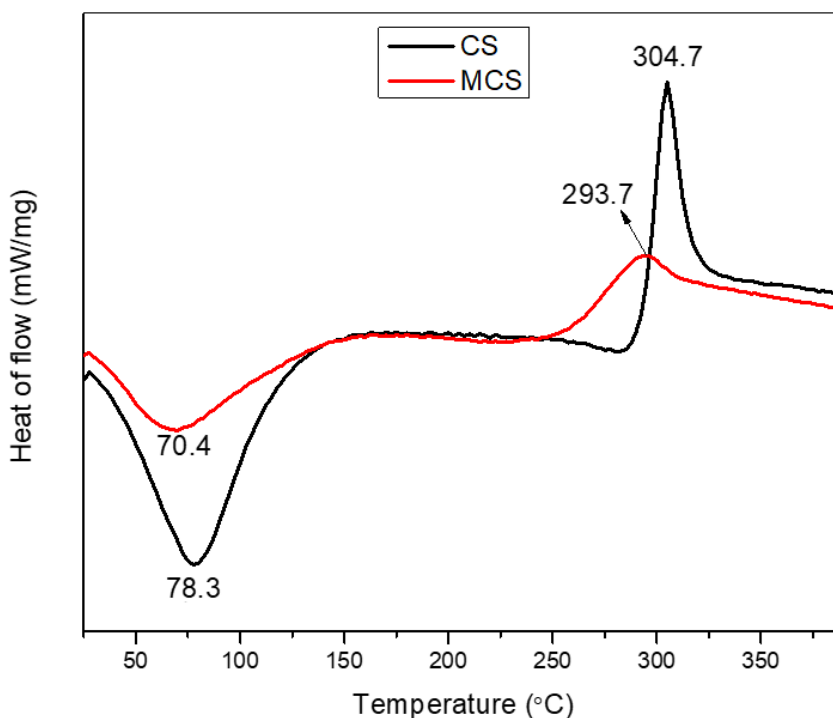


Figure 3.7. DSC plots of CS and MCS.

Due to the unsubstituted free -OH and -NH₂ groups of CS, this water is attached to the structure [122]. The breakdown of CS when heated is demonstrated by a clear, abrupt peak

at 304.7 °C, while for MCS, this characteristic peak occurs at 293.7 °C. These findings suggest that the degradation in MCS increased due to the chemical interaction of BPB with the CS matrix. Therefore, it is observed that MCS displays lower thermal stability compared to pure CS, aligning closely with the TGA results. The thermograms of MCS show changes in the breakdown and water volatilization temperatures, which are thought to be proof of the interaction between CS and BPB.

3.3.4. Study of antibacterial study

The results of the agar well diffusion test [98] for CS and MCS can be observed in Figure 3.8.

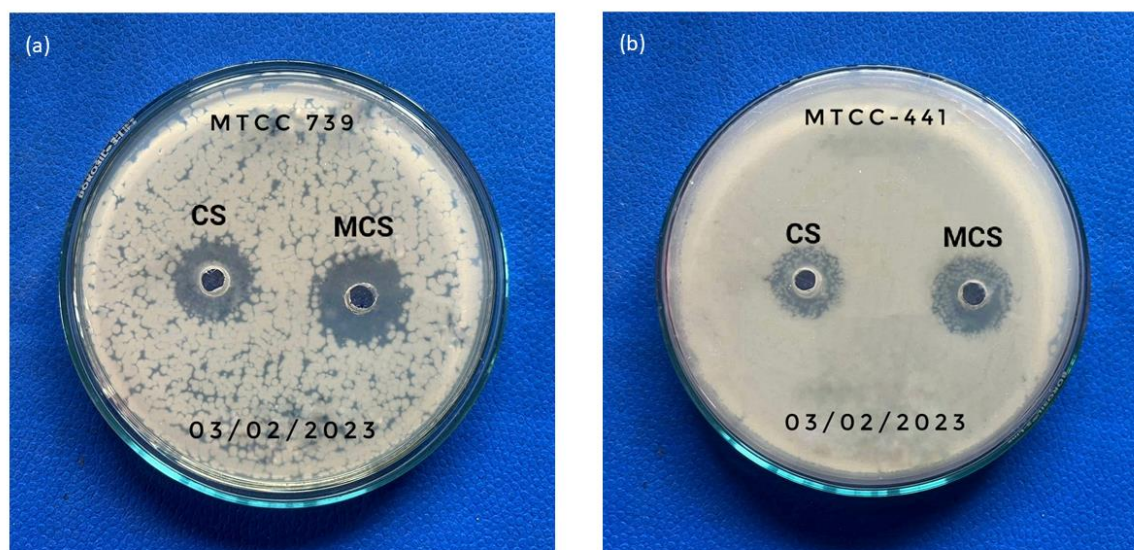


Figure 3.8. Antibacterial properties of CS and MCS on (a) *Escherichia coli* and (b) *Bacillus subtilis* bacteria.

The antibacterial assay was conducted on the test samples, namely CS and MCS, against two bacterial strains: *Escherichia coli* (MTCC-739), a gram-negative bacterium, and *Bacillus subtilis* (MTCC-441), a gram-positive bacterium, at a concentration of 10 mg mL⁻¹. The selection of a 10 mg mL⁻¹ concentration for the antibacterial test in the agar well diffusion method was based on the findings from the MIC method. Below this concentration, it was determined that inhibition did not occur, establishing 10 mg mL⁻¹ as the MIC. The detection of bacterial growth was based on the optical density measurements of the test samples, as illustrated in Figure 3.9. Certain inhibitory characteristics were also shown by the 2% acetic acid solution that was used to dissolve the test materials.

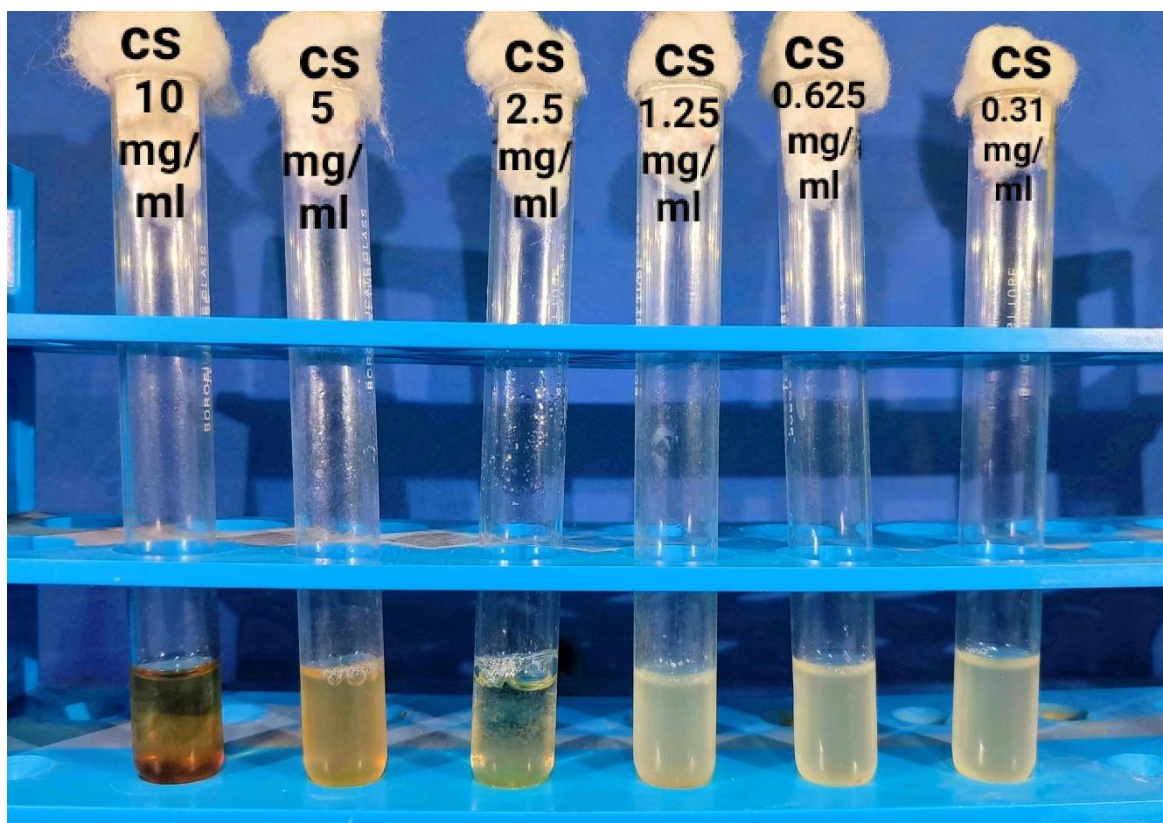


Figure 3.9. Antibacterial activities of CS against *Escherichia coli* bacteria via microdilution method for MIC.

Table 3.2. provides the zones of inhibition in the agar well method for the tested samples against a gram-negative and a gram-positive bacterium at a concentration of 10 mg mL⁻¹.

Table 3.2. Zone of inhibition observed in a test involving bacterial strains MTCC-739 and MTCC-441.

Sl. No.	Sample	Zone of inhibition (mm)	
		Gram negative bacteria	Gram positive bacteria
1.	CS	18 ± 0.01	16 ± 0.01
2.	MCS	20 ± 0.01	19 ± 0.01

For both cases involving MTCC-739 and MTCC-441, the inhibition was greater for MCS, measuring 20 mm and 19 mm, respectively, compared to pure CS, which recorded values of 18 mm and 16 mm, respectively. Additionally, it was also shown that gram-negative bacteria were more susceptible to the inhibitory effects of both CS and MCS than gram-positive

bacteria. The different cell wall architectures of gram-positive and gram-negative bacteria account for the observed differences in inhibitory efficacy against them. The cell walls of gram-positive and gram-negative bacteria are made of different peptidoglycan; gram-positive bacteria have peptidoglycan layers that are much thicker than those of gram-negative bacteria [118]. In general, gram-negative bacteria are more hydrophilic than gram-positive bacteria. Gram-negative bacteria have a higher hydrophilicity than gram-positive bacteria, which explains why the test samples were more sensitive to them and showed more noticeable morphological changes when treated [123].

3.3.5. Theoretical study

3.3.5.1. Geometry optimization and reaction mechanism

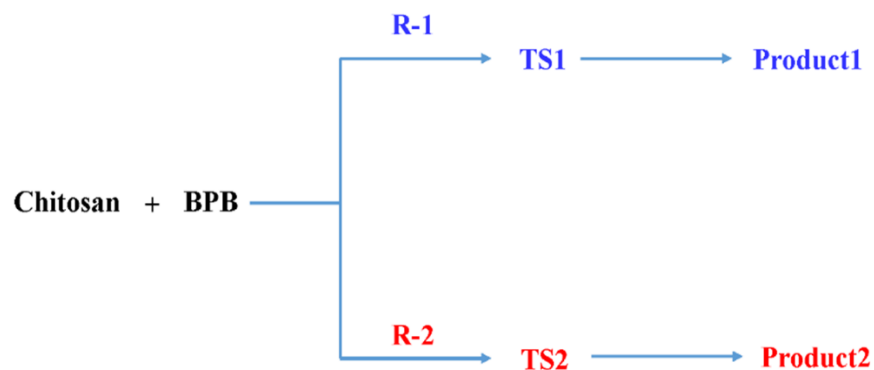
Computational investigation of reaction mechanisms is crucial for obtaining a more profound understanding of experimental observations. These studies have the potential to offer valuable insights into the nature of the products formed. In this work, the reaction of CS monomer and BPB is expected to proceed via a hydrogen abstraction reaction attached to the electronegative atom (oxygen and nitrogen). This leads to the bond formation between the electronegative atom of CS and the carbonyl carbon of BPB with the removal of hydrogen bromide (HBr). Two reaction mechanisms are proposed for the reaction:

- i.* Hydrogen abstraction from the primary hydroxyl group (R1).
- ii.* Hydrogen abstraction from the secondary hydroxyl group (R2).

The geometry optimization and frequency calculation of the species - reactants (R_n), transition states (TS_n), and products (P_n) ($n = 1, 2$) involved in the reaction mechanisms are carried out at the B3LYP/6-31G(d,p) level of theory. The transition states for each reaction channel were confirmed by the presence of only one negative frequency. The imaginary frequencies for TS1 and TS2 are 228.28 and 150.30 cm^{-1} , respectively. Moreover, the IRCs were also generated to confirm the reaction energy path connecting the reactants and products via corresponding transition states. Scheme 3.2. illustrates the suggested reaction pathway for the reaction between CS and BPB.

Similarly, Figure 3.10. displays the optimized structures of the species involved in the two reaction channels (R1, R2). The single-point energy at the DLPNO-CCSD(T)/def2-TZVP level of theory has been calculated by utilizing the optimized geometries obtained at the B3LYP/6-31G(d,p) level of theory. The single point calculation was performed using the

domain-based local pair natural orbital coupled-cluster theory with single, double, and perturbative triple excitations [DLPNO-CCSD(T)] level of theory with def2-TZVP basis set [107].



Scheme 3.2. Proposed reaction path for the reaction of CS with BPB.

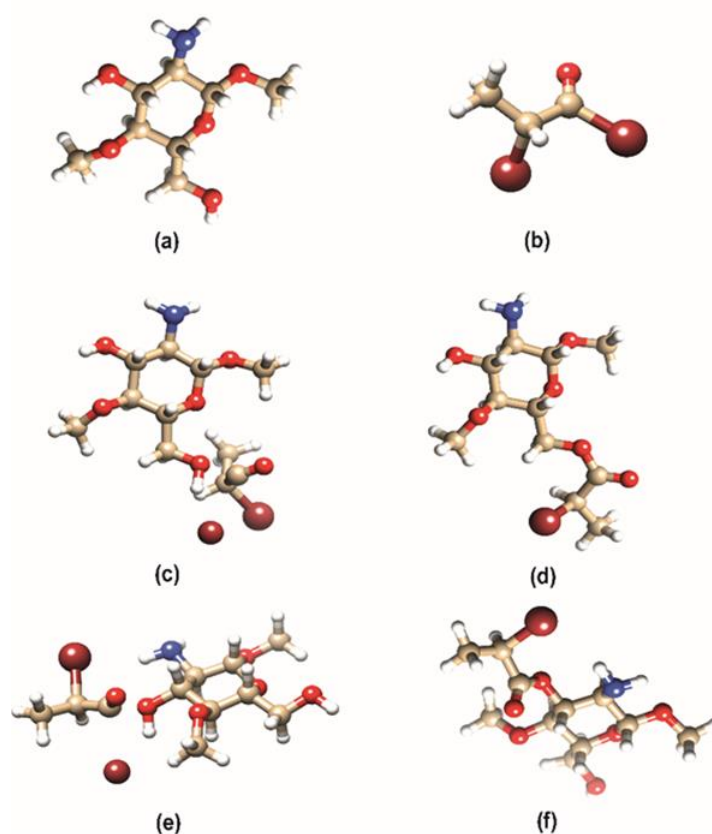


Figure 3.10. Optimized geometry of all the species for the reaction of CS with BPB at the B3LYP/6-31G(d,p) level of theory, where (a) and (b) are reactants (CS and BPB); (c) and (d) are TS1 and P1, respectively for R-1; and (e) and (f) are TS1 and P2, respectively for R-2.

3.3.5.2. Molecular electrostatic potential analysis

Molecular electrostatic potential (MEP) surface analysis has been performed to understand the total charge distribution in the molecule. This surface study helps in analysing the chemical reactivity of the reactants by predicting their active sites. The MEP surfaces are coloured differently based on the molecular charge distribution between +0.03 (deepest red) and -0.03 (deepest blue) and MEP maps of the reactants are given in Figure 3.11. The accompanying maps show the electron-deficient zone (electrophilic core) are represented in red colour, and the electron-rich zone (nucleophilic core) is represented in blue colour. In reactant 1, there are two major locations for nucleophilic attack or hydrogen abstraction, of which three are viable, as depicted in Figure 3.11. Likewise, for reactant 2, the carbonyl carbon is encircled by a red region, indicating an electron-deficient region. Overall, the presence of blue colour around the electronegative atom (reactant 1) and red colour around the carbonyl carbon (reactant 2) gives us a hint about the potential nucleophilic attack with the removal of HBr, which validates the selection of the proposed pathways. Thus, MEP analysis is necessary to determine the possible active sites of the reactants.

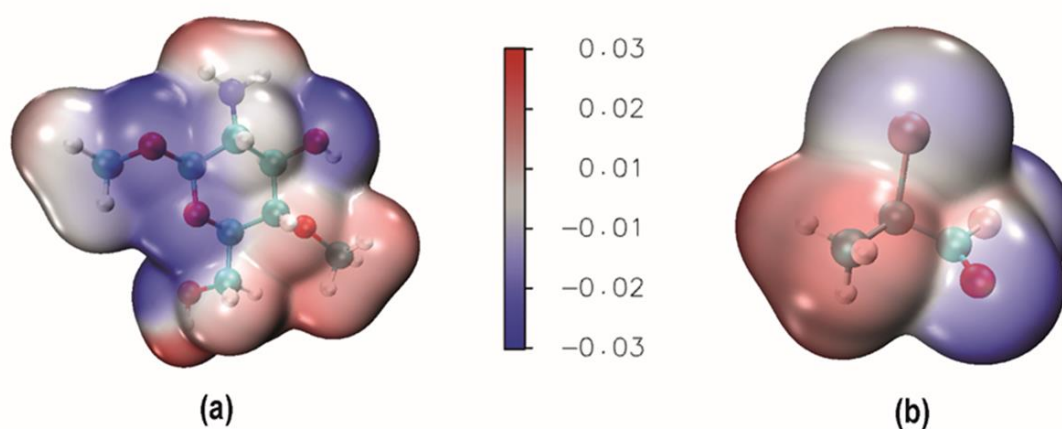


Figure 3.11. Three-dimensional MEP maps of (a) CS (b) BPB. The red and blue regions are the electron-deficient and electron-rich regions, respectively. Hetero atom colour codes: mauve = carbon; red = oxygen; blue = nitrogen; brown = bromine; and grey = hydrogen.

3.3.5.3. Energy profile diagram

The relative energy profile diagram (Figure 3.12.) of the reaction channels has been prepared at the DLPNO-CCSD(T)/def2-TZVP//B3LYP/6-31G(d,p) for the reaction channels. The

relative energies of the species have been tabulated in Table 3.3. For reference, we have set the energy of the reactants to be zero.

Table 3.3. Relative energies for the species of reaction channels 1 and 2 at the DLPNO-CCSD(T)/def2-TZVP//B3LYP/6-31G(d,p) level of theory. Energies are in kcal mol⁻¹.

Reaction Pathways	Species	Relative Energies
	Reactants	0.0
R-1	TS1	19.67
	P1	-7.87
R-2	TS2	15.93
	P2	-12.05

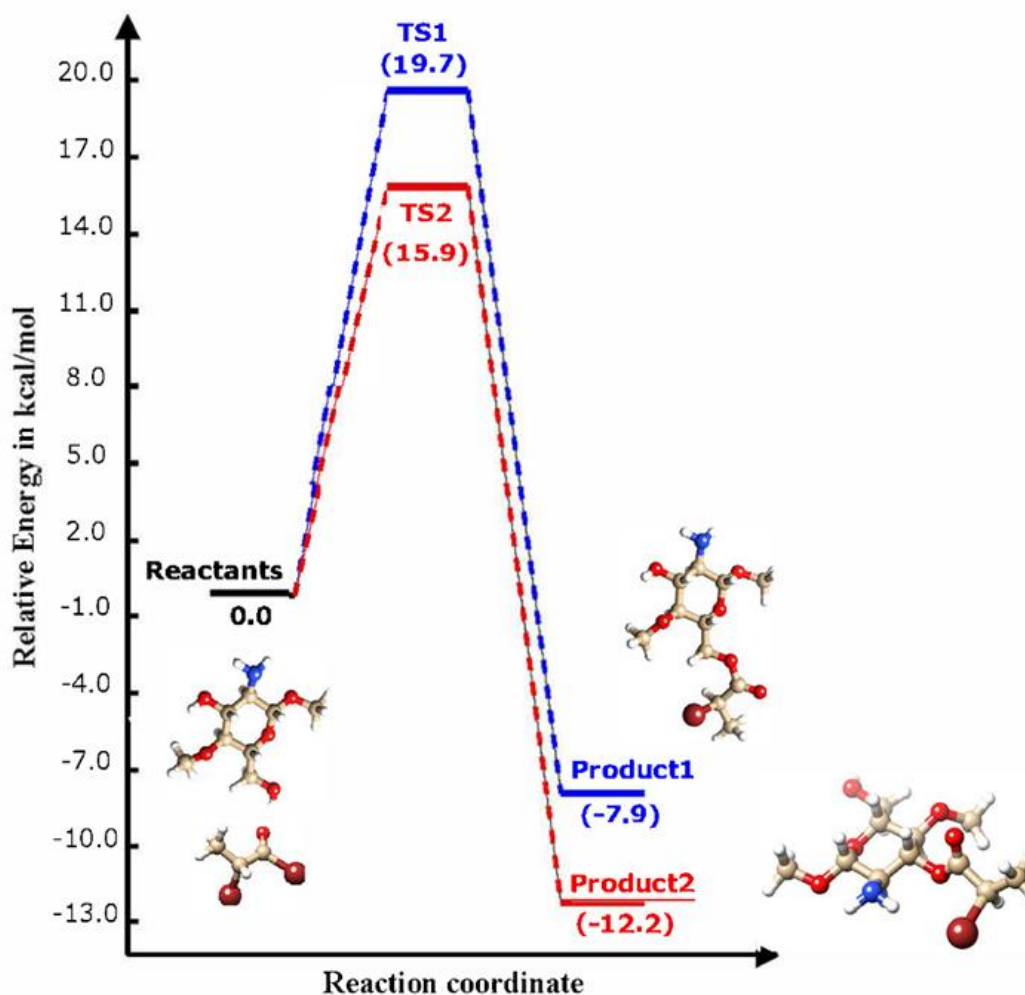


Figure 3.12. Relative energy profile for the reaction of CS and BPB obtained at the DLPNO-CCSD(T)/def2-TZVP//B3LYP/6-31G(d,p) level of theory. Blue colour represents R-1 reaction pathway and red colour represents R-2 reaction pathway.

From Figure 3.12., it can be seen that the reaction proceeds by the formation of transition states, TS_n ($n=1,2$) leading to the formation of products, P_n ($n=1,2$). For R-1, the barrier height is $19.7 \text{ kcal mol}^{-1}$ and the energy of the product is $-7.9 \text{ kcal mol}^{-1}$, with respect to the reactants. For R-2, the barrier height is $15.9 \text{ kcal mol}^{-1}$, and the products lie $-12.2 \text{ kcal mol}^{-1}$ below the energy of the reactants. From Figure 3.12., it can be inferred that P2 is both the kinetic (low barrier) as well as thermodynamic product (most stable).

3.3.5.3. Highest occupied molecular orbital and lowest unoccupied molecular orbital study

The highest occupied molecular orbital (HOMO) and lowest unoccupied molecular orbital (LUMO) play pivotal roles in quantum chemistry by elucidating a molecule's chemical reactivity and kinetic stability. The HOMO signifies the molecule's capacity to donate electrons while LUMO denotes its role as an electron acceptor. The pictorial representation of HOMO and LUMO frontier molecular orbitals of the products, P1 and P2 are shown in Figure 3.13. The positive and negative phases are represented in red and green, respectively. The plot clearly shows that in the two products, the HOMO molecular orbitals are predominantly localized on the Nitrogen atom of the CS molecule in P1 and P2. Additionally, the LUMO is distributed over the BPB molecule, highlighting its electron-accepting capability.

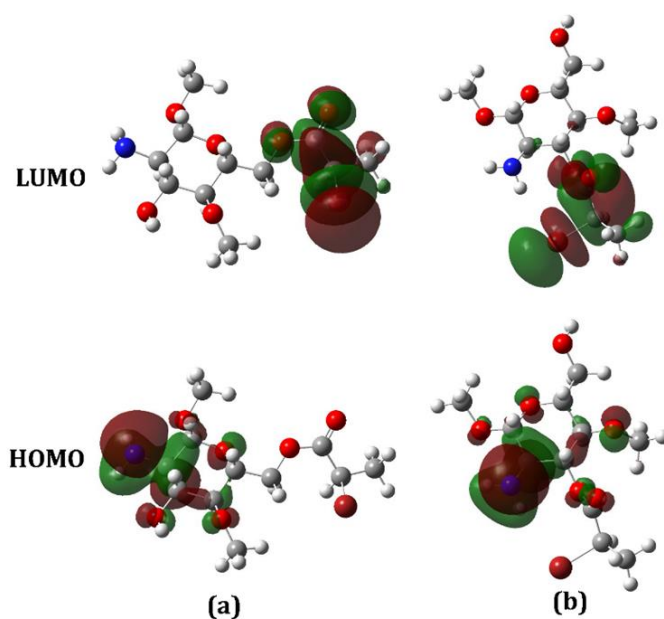


Figure 3.13. Frontier molecular orbitals (HOMO and LUMO) for the products, (a) P1 and (b) P2 of the reaction pathway, R-1 and R-2.

Using B3LYP functional, the quantum chemical investigation was performed for the two possible reaction pathways when the CS monomer reacted with BPB. The calculated IRC paths and energy barriers revealed that the product P2 of reaction R-2 is more likely to form.

3.4. Conclusion

In this study, the synthesis of MCS involved the reaction between CS and BPB in the presence of TEA and DMF. The characterization was conducted using FT-IR spectroscopy, UV/Vis spectroscopy, XRD, SEM, TGA, DSC, and NMR. FT-IR analysis indicates a shift in the absorption peak of the secondary -OH groups on the CS molecule to 1085 cm^{-1} . Additionally, the absorption peak of the primary amine group has moved to a lower wavenumber in the case of the MCS molecule. This suggests that the secondary -OH group and primary -NH₂ group of CS molecules underwent a reaction with BPB. Furthermore, in the case of MCS, a novel carbonyl peak appeared at 1742 cm^{-1} , signifying the successful grafting of BPB onto CS. MCS exhibits a wide UV/Vis absorption band spanning the wavelength range of 450-650 nm, a characteristic absent in CS. This observation underscores the occurrence of the reaction between CS and BPB. The XRD pattern verified that the inclusion of the BPB group brings about a modification in the crystallinity of CS. SEM micrographs revealed that the surface roughness of MCS was observed to be greater than that of pure CS. The interaction between the amine or hydroxyl groups of CS can account for this phenomenon. The introduction of the BPB group led to a decrease in thermal stability compared to pure CS, providing evidence of a notable chemical modification in CS. The presence of the reaction is confirmed by the decrease in thermal stability, which points to the formation of a chemical bond between these molecules. Additionally, the DSC study shows that the establishment of a chemical connection between CS and BPB resulted in a reduction in the thermal stability of MCS. The NMR study implies the existence of the carbonyl carbon from BPB, potentially suggesting grafting through the N-atom. The antibacterial activity of both CS and MCS was examined, revealing greater inhibition for MCS compared to pure CS with regard to both gram-positive and gram-negative bacteria. Employing the B3LYP functional, a quantum chemical investigation was conducted to explore the two potential reaction pathways when the CS monomer reacts with BPB. The calculated IRC paths and energy barriers indicate that the formation of product P2 in reaction R-2 is more likely to occur. Therefore, all the analyses collectively indicate that the reaction between CS and BPB has indeed taken place. FT-IR and SEM analyses suggest that the secondary -OH group and primary -NH₂ group of CS molecules underwent a reaction with

BPB. Additionally, NMR analysis indicates the presence of carbonyl carbon from BPB, possibly through the N-atom. The theoretical study indicates that both the primary and secondary -OH groups of CS molecules have the potential to undergo a reaction with BPB, but it is more likely that the reaction with the secondary -OH group will occur. In conclusion, it can be affirmed that the BPB group can undergo grafting onto CS through the primary O-atom, secondary O-atom, and primary N-atom.